DEVELOPMENTAL DYNAMICS 247:1121–1134, 2018
DOI: 10.1002/DVDY.24669

RESEARCH ARTICLE

Endochondral Ossification in Hindlimbs During *Bufo gargarizans* Metamorphosis: A Model of Studying Skeletal Development in Vertebrates

Jinshu Gao, Xinyi Li, Yuhui Zhang, and Hongyuan Wang*

College of Life Science, Shaanxi Normal University, Xi'an, 710119, China

Background Endochondral ossification, the process by which most of the skeleton is formed, is accurately regulated by many specific groups of molecules and extracellular matrix components. The molecular mechanisms of endochondral ossification have been extensively investigated in mammals. However, there are few studies about it in amphibians. **Results** Ossification of femur and tibiofibula was observed at Gs 40, and tarsals and metatarsals were ossified at Gs 42. Most of the skeletons in hindlimbs were completely ossified except for articular cartilages at Gs 46. Thirty-two genes related to endochondral ossification were found in the differentially expressed genes (DEGs) library of hindlimbs, and nine of these genes were validated by qRT-PCR during metamorphosis. Sox9 was expressed in the columnar, prehypertrophic, and upper hypertrophic zones, and the expression of Ihh was observed in prehypertrophic chondrocyte zone in hindlimbs of *B. gargarizans*. **Conclusions** The ossification of hindlimbs increased gradually, and the ossification sequence was from proximal to distal in *B. gargarizans* during metamorphosis. Thirty-two genes found in the DEGs library were related to the regulation of endochondral ossification of hindlimbs in amphibians. The present study will provide a valuable genomic resource for the future study of endochondral ossification in amphibian. *Developmental Dynamics* 247:1121–1134, 2018. © 2018 Wiley Periodicals, Inc.

Key words: Endochondral ossification; hindlimbs; development; Sox9; Ihh

Submitted 28 May 2018; First Decision 22 August 2018; Accepted 22 August 2018; Published online 11 October 2018

Introduction

Amphibian metamorphosis is a classic model to study the developmental transition from aquatic to terrestrial existence of vertebrates. During metamorphosis, most of the amphibians undergo a major developmental transition that involves dramatic morphological and physiological changes, including organ resorption, de novo development, and organ and tissue remodeling that prepare the organism for the adult life (Nakai et al., 2016; Kulkarni and Gramapurohit, 2017). In particular, de novo development of the hindlimbs and forelimbs is critically important for amphibians due to their roles in assisting in the terrestrial locomotion and adjusting to the terrestrial life (Brown and Cai, 2007; Wang et al., 2015).

The ossification of amphibian limb bone exhibits a specific sequence and shares the conservative patterns. Sequence of limb ossification generally proceeds from proximal to distal (Erdmann, 1933; Wiens, 1989; Haas, 1999; Banbury and Maglia, 2006; Gao et al., 2015). Endochondral ossification plays critical roles in early limb patterning and skeletal growth (Nishimura et al., 2012). Due to the property of easily observing the process of ossification during amphibian metamorphosis by double-staining methodology, limb in tadpoles offered an excellent model to gain insight into the molecular mechanisms that regulate endochondral ossification. During endochondral ossification, mesenchymal cells initially differentiate into mitotic chondrocytes that deposit extracellular matrix to form cartilage elements. Following proliferation, mitotic chondrocytes pass through a transition stage at which they are known as prehypertrophic chondrocytes. Prehypertrophic chondrocytes differentiate into hypertrophic chondrocytes, eventually undergoing cell death and leaving a matrix that is converted to bone by invading osteoblasts. (Mackie et al., 2008; Ohba et al., 2015). In addition, several studies suggested that hypertrophic chondrocytes can become osteoblasts in endochondral bone formation (Yang et al., 2014; Zhou et al., 2014).

To date, the molecular mechanisms of endochondral ossification have been extensively investigated in mammals (Karp et al., 2000; Bird and Mabee, 2003; Wongdee et al., 2013; Ohba et al., 2015). Endochondral ossification, a complex and unique biological event, requires coordinated interplay of many specific groups of molecules and extracellular matrix components (Mackie et al., 2008; Nishimura et al., 2012). Several systemic factors, transcription factors, and locally secreted factors, including SRY-box containing gene9

Grant sponsor: National Natural Science Foundation of China; Grant number: 31572222; Grant sponsor: Shaanxi Normal University; Grant numbers: GK201703037 and GK201703039.
*Correspondence to: Hongyuan Wang, College of Life Science, Shaanxi Normal University, Xi'an 710119, P.R. China. E-mail: hongyuanwang@snnu.edu.cn

Article is online at: http://onlinelibrary.wiley.com/doi/10.1002/dvdy.24669/abstract

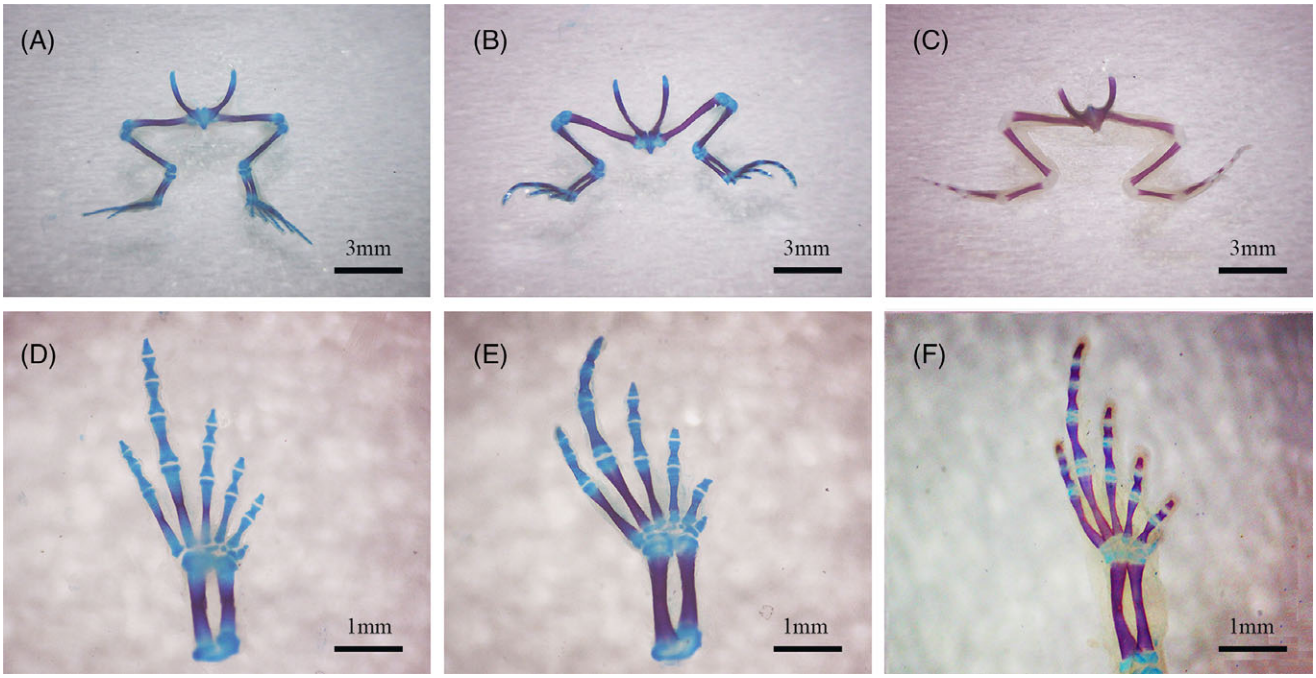

Fig. 1. Double-stained skeletons of the hindlimbs of *B. gargarizans* during metamorphosis, exhibiting cartilages (blue) and bones (red). Dorsal views of the whole hindlimbs at Gs 40 (**A**), Gs 42 (**B**), and Gs 46 (**C**), respectively. Magnification of the metatarsals of hindlimbs at Gs 40 (**D**), Gs 42 (**E**), and Gs 46 (**F**), respectively.

(Sox9), bone morphogenetic proteins (BMPs), Indian hedgehog (Ihh), fibroblast growth factors (FGFs), parathyroid-related protein (PTHrP), and insulin growth factor, are involved in this complex regulation of endochondral ossification (Gómez et al., 2017). The existence of complex cross talk among these factors in the regulation of chondrocyte proliferation and hypertrophy during endochondral ossification were well confirmed (Moriishi et al., 2005; Nishimura et al., 2012). Unfortunately, there are few studies about the molecular mechanisms of endochondral ossification in amphibians at present.

Bufo gargarizans belongs to *Bufonidae Bufo* and is a species of toad endemic to China (Sun et al., 2015). It is widely distributed from China to Russia and in Korea. *B. gargarizans* is considered a species of "least concern" in the recent IUCN Red List (http://www.iucnredlist.org/), suggesting that the population of this common species is stable. Their embryo and larval stages take place in water, and adult stages take place on land. In addition, their shorter breeding cycle makes it convenient to collect samples from different developmental stages in a short period. In addition, during larval stages, the identification of Gosner stages (Gs) (Gosner, 1960) is based on the development degree of hindlimbs. Thus, *B. gargarizans* is an excellent model to study the mechanisms of endochondral ossification in hindlimbs during the metamorphosis.

In the present study, hindlimb skeletons at different developmental stages of *B. gargarizans* tadpole were investigated using double-staining method. Then, Illumina transcriptome sequencing technology was applied to perform the comprehensive transcriptome of hindlimbs in *B. gargarizans*. Also, quantitative real-time polymerase chain reaction (qRT-PCR) and in situ hybridization were conducted to validate the mRNA level of selected genes and to identify the location of the Sox9 and Ihh mRNA in hindlimbs, respectively. The present study might provide new insights into complex molecular mechanisms in regulation of endochondral ossification.

Results

Development of Hindlimbs

The *B. gargarizans* hindlimb is composed of the femur, tibiofibula, fused tibiale and fibulare, distal tarsale 3-2, distal tarsale 1, metatarsalia V–I, and phalanges arranged in the typical formula 3-4-3-2-2, and the prehallux is formed by two elements (Fig. 1) (Gao et al., 2015). By the end of metamorphosis (Gs 46), hindlimb bones were completely ossified except for articular cartilage compared to the partial ossification of hindlimb bones at Gs 40 and Gs 42. Specifically, ossification of diaphyses first began in femur, then in tibiofibula, then in metatarsals. The femur was ossified partially at Gs 40, and it was ossified completely at Gs 42 (Fig. 1A,B). By stage 40, the tibiofibula was not fused, and the diaphyses were ossified slightly (Fig. 1A). In addition, phalangeal formulae for the hindlimbs from toe I to toe V was formed, while the metatarsals III–IV were ossified slightly at Gs 40 (Fig. 1D). The tibiofibula was completely fused, and their diaphyses were fully ossified at Gs 42. In addition, the metatarsals III–V began to fully ossify at Gs 42 (Fig. 1E). Finally, most of the elements except for articular cartilages were fully ossified at Gs 46 (Fig. 1F).

RNA sequencing, Unigene Assembly, and Annotation

To comprehensively analyze the transcriptomes of *B. gargarizans* hindlimbs (including skin, muscle, perhaps nerve, and other tissues besides endochondral tissue) over different developmental stages, four cDNA libraries were created and sequenced using the Illumina HiSeq 2500 platform. The two lanes of Illumina sequencing generated a total of 197,931,422 raw reads, which was reduced to 165,879,590 high-quality reads with 90% Q30 percentages (1% sequencing error rate) after filtering the sequence for low-quality reads (Table 1). We assembled these high-quality reads into 92,682 unigenes using a de novo assembly with Trinity (Table 1) (Haas et al., 2013). The length

TABLE 1. Summary of the Sequencing and Assembly of the *B. gargarizans* Transcriptome

	Raw reads	Clean reads	Q30%†	Bases (bp)
Hindlimbs (Gs 40)	49,970,846	42,682,256	93.09	6,224,492,735
Hindlimbs (Gs 42)	48,512,230	40,394,822	84.03	5,812,012,233
Tail (Gs 40)	49,784,942	41,490,780	92.43	6,038,345,057
Hindlimbs (Gs 46)	49,663,404	41,311,732	92.82	6,021,159,181
Total raw data	197,931,422			
Total high-quality data	165,879,590			
Total unigene length (bp)	99568914			
Average unigene length (bp)	1074.30			
N50 (bp)	1449			

†Q30%: The proportion of nucleotides with quality value > 30.

TABLE 2. Overview of the Annotated Unigenes

Database	Total unigenes	Annotated unigenes	Percent (%)
NR	92682	45844	49.46%
GO	92682	42383	45.73%
COG	92682	41663	44.95%
KEGG	92682	19895	21.47%

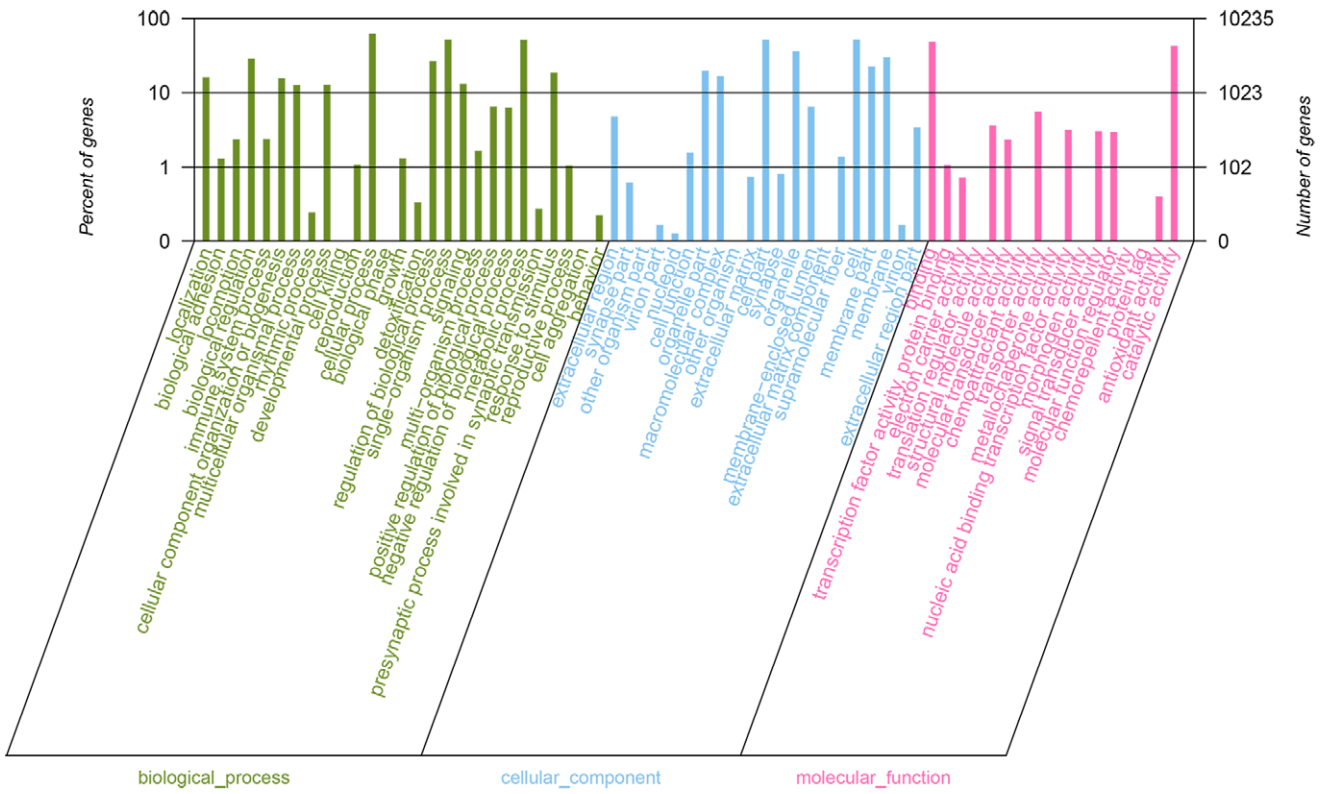

Fig. 2. Histogram presentations of GO classification of the unigenes of the transcriptome of *B. gargarizans*. The right *y*-axis indicates the number of genes in the category; the left *y*-axis indicates the percentage of a specific category of genes in that main category.

of unigenes ranged from 200 bp to 3 kb, with average and total lengths of 1074 bp and 99.6 Mb, respectively (Table 1).

To validate and annotate the assembled transcripts from transcriptome, the unigenes were annotated based on sequence similarities to genes in the database of NCBI-nr, GO, COG, and KEGG using BLASTx with an e-value cutoff of at or below 1e−5. We had annotation rates of 49.46 % (45,844) for NR, 45.73 % (42,383) for GO, 45.95 % (41,663)

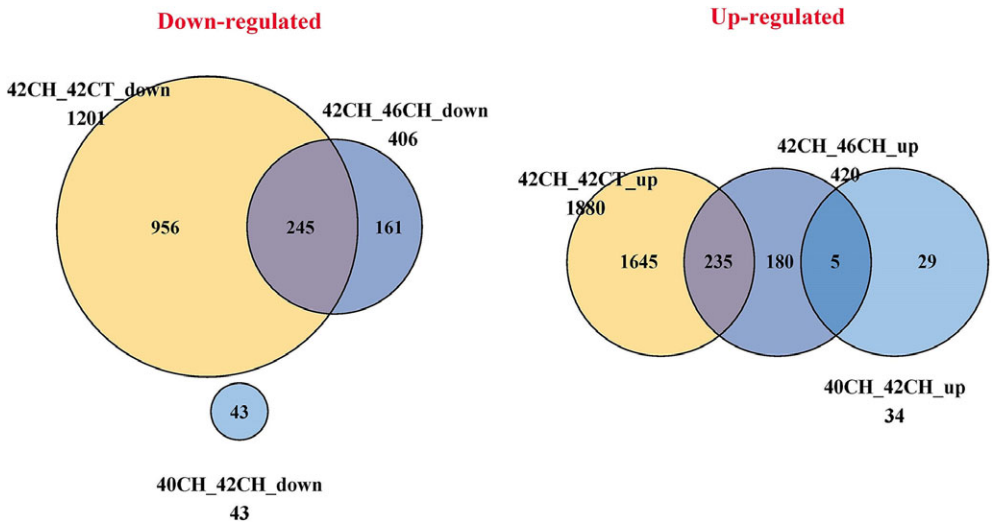

Fig. 3. Venn diagrams showing the unique and shared DEGs (down-regulated and up-regulated genes) among the four cDNA libraries: 40CH, 42CH, 42CT, and 46CH refered to hindlimbs of *B. gargarizans* at Gs 40, hindlimbs at Gs 42, tail at Gs 42, and hindlimbs at Gs 46, repectively. Down-regulated means that the gene expression of the former was higher than that of the latter, and up-regulated means that the gene expression of the former was lower than that of the latter. For example, 42CH_42CT_down 1201 means that the expression of 1201 genes was down-regulated in the tail at Gs 42 (42CT) compared with those of the hindlimbs at Gs 42 (42CH).

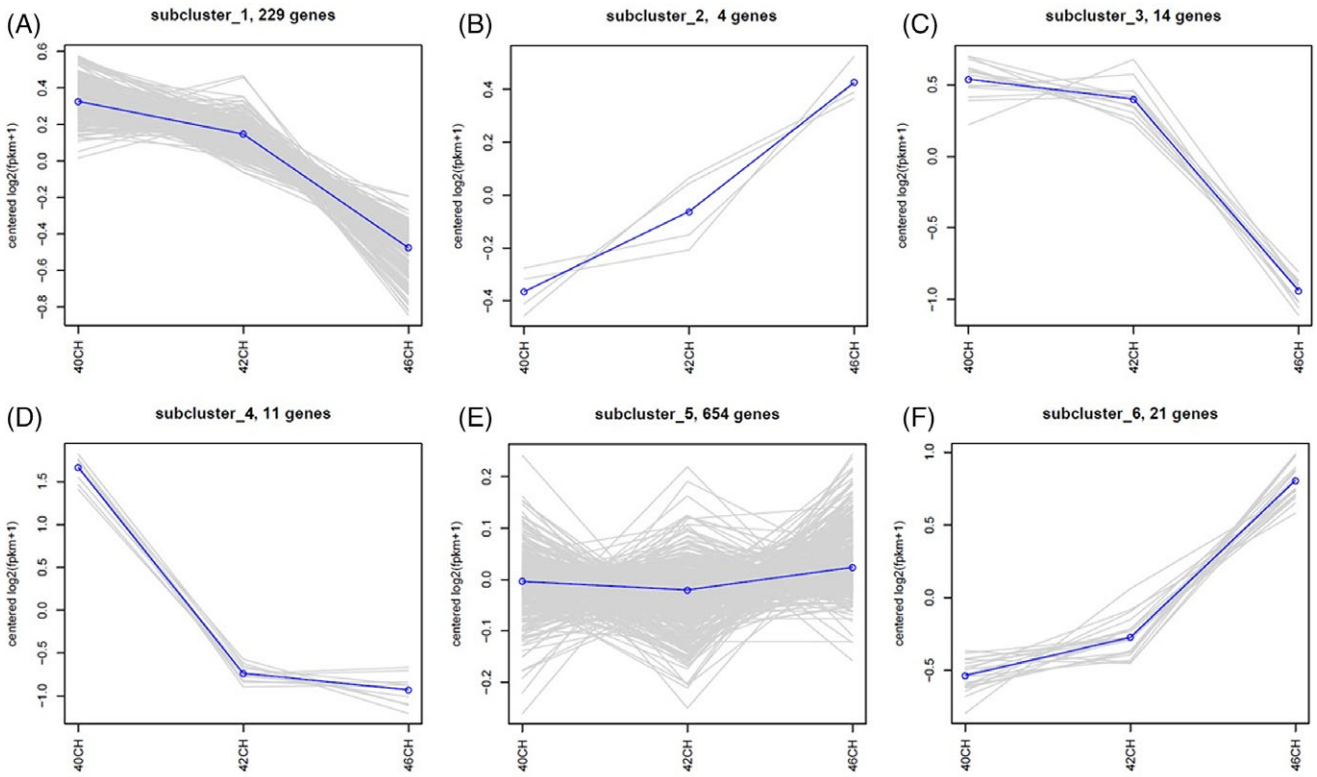

Fig. 4. Developmental trajectories of six gene clusters classified with differential expression profiles during metamorphosis of *B. gargarizans*.

for COG, and 21.47 % (19,895) for KEGG database, respectively (Table 2).

Unigenes Functional Classification

A further classification of functional genes was also performed against the gene ontology (GO) databases. GO, an international and standardized gene functional classification system, was used to predict the unigene functions at the macro level, which covers three domains: cellular component, molecular function, and biological process. The GO classification results showed that biological process classification was mainly concentrated in cellular process (62.35%) and metabolic process (51.35%). In addition, the dominant categories were cell (51.91%) and cell part

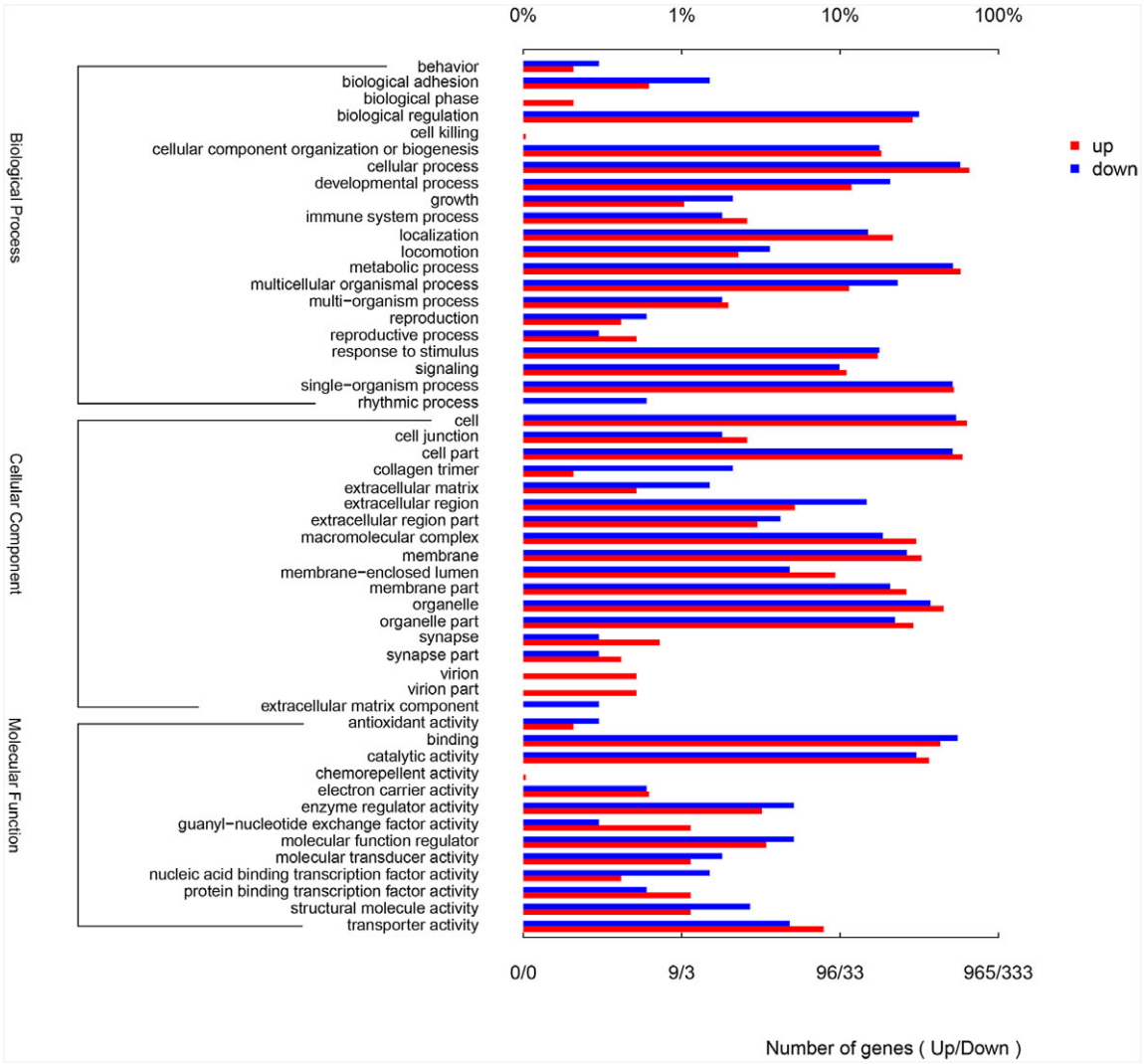

Fig. 5. The representative GO terms enriched by differently expressed genes between tail and hindlimbs of *B. gargarizans* at Gs 42.

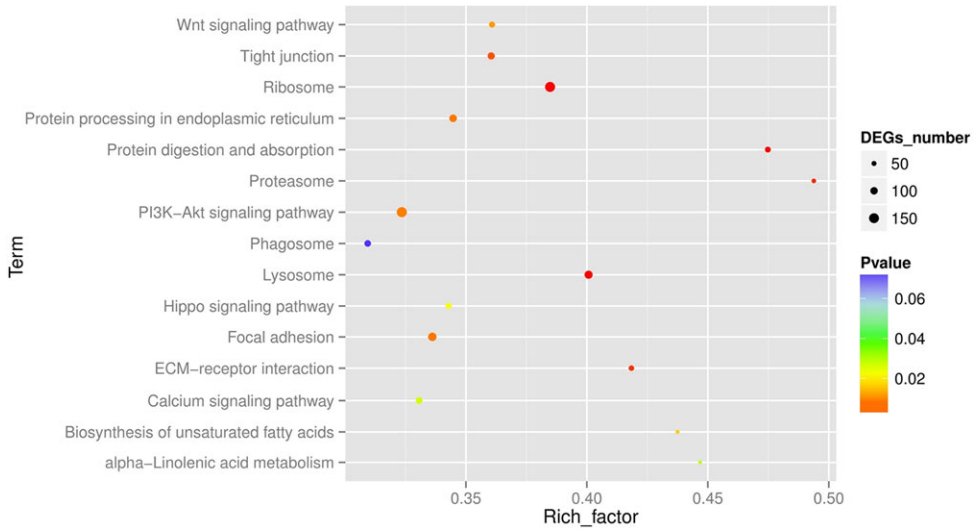

Fig. 6. Scatterplot of enriched KEGG pathways for DEGs between tail and hindlimbs of *B. gargarizans* at Gs 42. The *y*-axis represents the KEGG pathways, and the *x*-axis represents the Rich factor (that is, the ratio of the number of DEGs enriched in the pathways to the number of annotated genes. The higher the Rich factor, the greater the degree of enrichment). The size of the dot indicates the number of DEGs in the pathway, and the color of the dot corresponds to different Q values.

TABLE 3. Genes Related to the Endochondral Ossification

ID	Gene	Product	RPKM			
# Systemic factors			Hindlimbs (Gs 40)	Hindlimbs (Gs 42)	Tail (Gs 42)	Hindlimbs (Gs 46)
TRINITY_DN41910_c0_g2	D1	Type I iodothyronine deiodinase	1.27	0.46	0.64	0.19
TRINITY_DN77067_c0_1	D2	Type II iodothyronine deiodinase	32.57	34.65	5.12	8.46
TRINITY_DN18629_c0_g1	D3	Type III iodothyronine deiodinase	3.21	7.64	79.75	11.42
TRINITY_DN72355_c2_g4	TRα	Thyroid hormone receptor alpha	4.1	2.39	1.32	1.94
TRINITY_DN61740_c0_g1	TRβ	Thyroid hormone receptor beta	4.35	3.33	1.93	0.69
TRINITY_DN74736_c0_g1	GHR	Growth hormone receptor	5.41	8.64	2.15	5.28
TRINITY_DN73623_c0_g2	LR	Leptin receptor	0	3.32	0	0.79
TRINITY_DN65590_c3_g1	RXR	retinoid X receptor beta L homeolog	38.9	41.39	51.79	40.08
# Transcription factors						
TRINITY_DN75037_c0_g2	Sox9	SRY-box-containing gene 9	44.82	49.71	5.20	72.25
TRINITY_DN74876_c5_g2	MEF2C	Myocyte enhancer factor-2	42.73	48.73	5.99	25.97
TRINITY_DN73644_c0_g1	Runx1	Runt-related transcription factor 1	4.58	4.71	5.82	2.59
TRINITY_DN67992_c0_g1	Runx2	Runt-related transcription factor 2	1.70	4.55	5.62	6.12
TRINITY_DN42241_c0_g1	Runx3	Runt-related transcription factor 3	1.26	0.46	0.28	0.20
# Locally produced factors						
TRINITY_DN66576_c0_g2	Ihh	Indian hedgehog protein	26.86	16.78	3.40	15.76
TRINITY_DN66200_c0_g1	HHAT	Hedgehog acyltransferase	38.33	43.63	112.48	119.95
TRINITY_DN70160_c0_g1	Wnt9b	Wingless-type MMTV integration site family member 9b	1.47	1.60	0.53	1.99
TRINITY_DN36306_c0_g1	Wnt10b	Wingless-type MMTV integration site family member 10b	13.22	14.76	7.05	9.48
TRINITY_DN51506_c0_g1	BMP6	Bone morphogenetic protein 6	5.10	7.00	1.06	7.46
TRINITY_DN71381_c1_g4	BMP7	Bone morphogenetic protein 7	16.36	14.40	8.73	12.89
TRINITY_DN75978_c0_g1	PTH/ PTHrPR	Parathyroid hormone-related peptide receptor	17.83	14.85	0.27	11.55
TRINITY_DN40319_c0_g2	FGFBP3	Fibroblast growth factor-binding protein 3	65.61	42.10	5.54	27.22
TRINITY_DN59633_c0_g1	FGF9	Fibroblast growth factor 9	0.73	1.20	0.80	0.83
TRINITY_DN59231_c0_g1	FGF16	Fibroblast growth factor 16	2.39	2.02	0.50	1.25
TRINITY_DN76881_c2_g1	TGFβ	Transforming growth factor beta	6.00	6.31	2.11	3.38
TRINITY_DN76381_c1_g1	TGFRβ	Transforming growth factor beta receptor	12.49	22.75	2.90	19.55
TRINITY_DN13688_c0_g1	VEGF-A	Vascular endothelial growth factor A	0	1.53	0	0
TRINITY_DN55551_c0_g1	VEGF-B	Vascular endothelial growth factor B	2.50	0.52	3.30	0.94
TRINITY_DN50830_c1_g1	VEGF-C	Vascular endothelial growth factor C	1.57	3.09	3.74	1.40
TRINITY_DN75003_c0_g1	VEGFR-1	Vascular endothelial growth factor receptor 1	1.65	1.26	0.14	0.38
TRINITY_DN75777_c0_g1	VEGFR-2	Vascular endothelial growth factor receptor 2	3.63	3.03	1.39	1.23
TRINITY_DN58865_c3_g1	CY2	Alpha1 type II collagen	3571.73	4854.14	101.48	3956.87
TRINITY_DN62188_c2_g1	MMP9	Matrix metalloproteinase-9	19.49	25.37	123.60	57.87

(51.65%) in the cellular component ontology, and binding (48.44%) and catalytic activity (42.55%) in the molecular function ontology (Fig. 2).

Identification of Differential Gene Expression

To identify DEGs between tail and hindlimbs at Gs 42, and among hindlimbs of different developmental stages in *B. gargarizans*, pairwise comparisons were conducted and the DEGs were extracted using EBSeq software set at two stringency levels (FDR < 0.05 and $|Log_2FC|>1$) (Robinson et al., 2010). In all, 2094 and 1405 unigenes were significantly up- and down-regulated, respectively (Fig. 3). For the pairwise comparisons among the four cDNA libraries, we detected 1201 (42CH vs. 42CT), 43 (40CH vs. 42CH), and 406 (42CH vs. 46CH) down-regulated DEGs; 1880 (42CH vs. 42CT), 34 (40CH vs. 42CH), and 420 (42CH vs 46CH) up-regulated DEGs were also observed (Fig. 3).

Differential gene expression patterns in *B. gargarizans* hindlimbs during metamorphosis were then clustered based on the standardized fragments per kilobase of exon per million reads

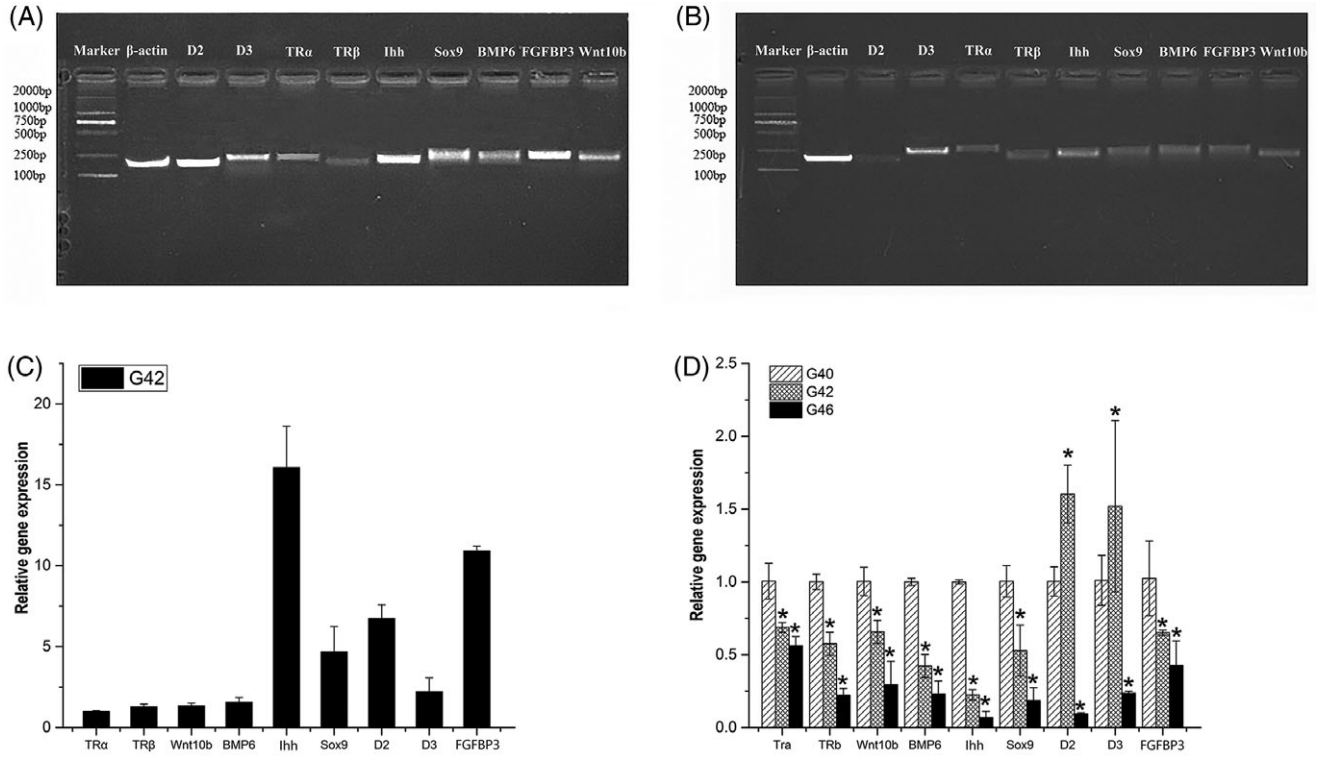

Fig. 7. Validation of nine unigenes by semiquantitative RT-PCR and qRT-PCR. Gel images of semiquantitative RT–PCR analysis of nine unigenes in *B. gargarizans* hindlimbs (**A**) and tails (**B**) at Gs 42. β-actin was used as internal standard for RT–PCR. The migration of DL2000 DNA marker is shown on the left side. **C**: Relative expression of genes in hindlimbs of *B. gargarizans* at Gs 42 using qRT-PCR. **D**: Relative expression of genes in hindlimbs of *B. gargarizans* at Gs 40, Gs 42, and Gs 46 using qRT-PCR. The values are expressed in mean ± SD (n = 3). Asterisks indicate significant difference compared to control, $^*P < 0.05$. The full names of minor nomenclature about genes involved in pictures are shown in Table 3.

mapped (FPKM) and were divided into six clusters (Fig. 4). Each cluster represented gene-expression trajectories in either increasing or decreasing patterns across development. In clusters, a total of 254 uingenes were high-expressed at Gs 40 (Fig. 4 A,C, D). In addition, in the Gs 46–specific high-expression cluster, 25 unigenes were observed (Fig. 4 B,F).

Functional Enrichment Analysis of Differentially Expressed Genes

To gain insight into the functional distribution of genes that differentially expressed in tail and hindlimbs of *B. gargarizans* at Gs 42, we linked all DEGs in tail and hindlimbs at Gs 42 to the enriched GO terms to look for components that could be grouped based on the broad GO categories. The results showed that each DEG could be assigned to more than one GO term, and a total of 679 genes were classified into biological process, followed by cellular component (413 genes) and molecular function (200 genes). In the biological process classes, the predominant subfamily was cellular process, followed by single-organism process and metabolic process. For the cellular component classes category, cell part and organelle were the main groups. In addition, among the molecular function, the binding was prominently enriched, next to catalytic activity and transporter activity (Fig. 5). These results suggested that tail and hindlimb development involve totally different processes.

To further analyze the biochemical pathways of the DEGs, they were mapped to the terms in the KEGG database and compared with the whole transcriptome background. KEGG is a database resource for understanding high-level functions and utilities of the biological system, such as the cell, the organism, and the ecosystem, from molecular-level information. KEGG analysis of the tail and hindlimbs at Gs 42 resulted in 3081 sequences of the DEGs being classified into 328 different pathways. The top 15 significant enrichment pathways are shown in Figure 6. Among these, PI3K-Akt signaling pathway was the most enriched, and 140 genes were enriched in this pathway. In addition, other pathways were mainly classified into Ribosome, Lysosome, Focal adhesion and Tight junction.

The Expression Profiles of Genes Related to the Endochondral Ossification

It has been known that systemic factors, transcription factorsm and locally secreted factors play important roles in the regulation of chondrocyte proliferation and hypertrophy during endochondral ossification. Based on the annotation results, eight systemic factors—D1, D2, D3, TRα, TRβ, GHR, LR, and RXR—were identified. Most of these genes were expressed at high levels in hindlimbs at Gs 42 compared to the expression in tail at Gs 42 (Table 3). The mRNA expression of D2 and GHR were up-regulated and peaked in hindlimbs at Gs 42, while down-regulated at Gs 46. With the development of hindlimbs, there was a decrease in the D1, TRα, and TRβ mRNA levels. In contrast, the mRNA of D3 monotonically increased with the development. The RXR expression had no obvious changes in hindlimbs among different developmental stages of *B. gargarizans*. Notably, LR was expressed in hindlimbs only at Gs 42. As transcription factors,

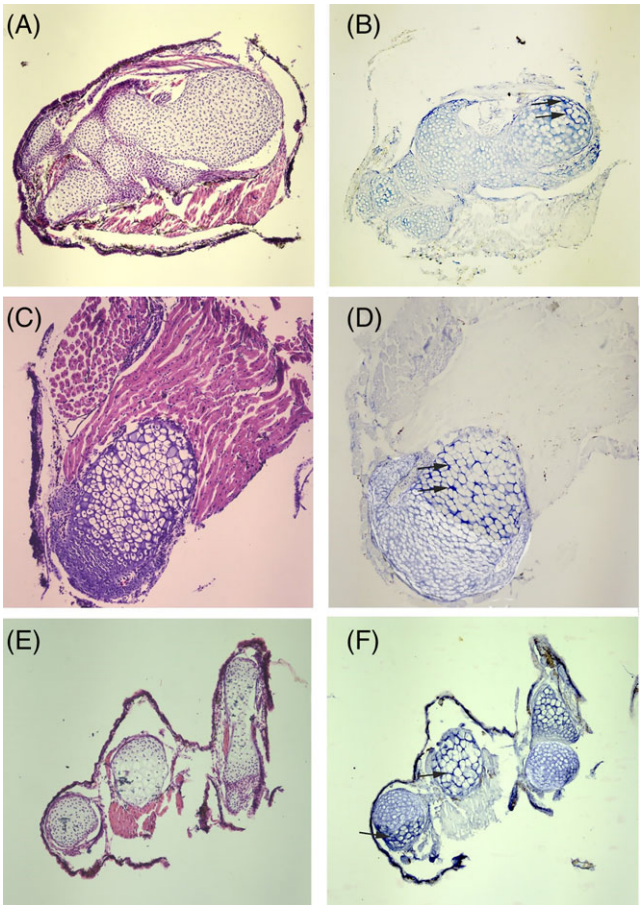

Fig. 8. Expression of Ihh mRNAs in hindlimbs of *B. gargarizans* among different developmental stages determined by in situ hybridization. **A,C, E** show sections stained with H&E; **B,D,F** show sections hybridized with an Ihh antisense probe. Arrows in B,D,F show positive cells in the growth cartilage; A,B, femur at Gs 40; C,D, femur at Gs 42; E,F, tibiofibula at G46.

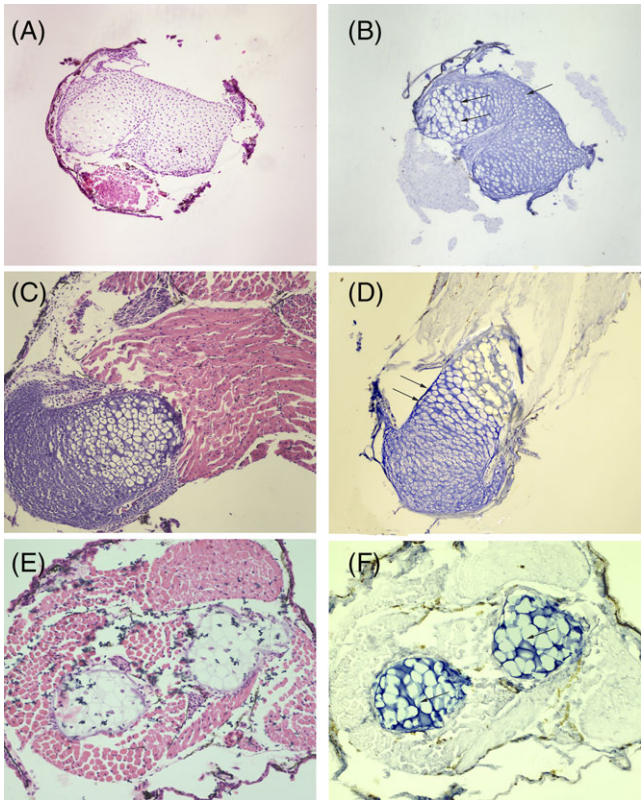

Fig. 9. Expression of Sox9 mRNAs in hindlimbs of *B. gargarizans* among different developmental stages determined by in situ hybridization. **A,C, E** show sections stained with H&E and pictures **B,D,F** show sections hybridized with a Sox9 antisense probe. Arrows in B,D,F show positive cells in the growth cartilage; A,B, femur at Gs 40; C,D, femur at Gs 42; E,F, tibiofibula at G46.

five genes related to regulation of skeletal development were identified, which were differentially expressed over the developmental stages. Three of the five transcription factors were expressed higher in hindlimbs than in tail at Gs 42. In addition, a total of 19 genes related to locally produced factors were identified from the unigene sequences. Among these genes, Wnt10b, FGF9, TGFβ, TGFRβ, VEGF-C, and CY2 were up-regulated and peaked in hindlimbs at Gs 42. In addition, the mRNA expression of Ihh, BMP7, PTH/PTHrPR, FGFBP3, FGF16, VEGFR-1, and VEGFR-2 were down-regulated in hindlimbs with the development, while the expression of HHAT, Wnt9b, BMP6, amd MMP9 were up regulated. Notably, VEGF-A was expressed in hindlimbs only at Gs 42.

Validation of DEGs by Using qRT-PCR

Quantitative real-time RT-PCR and semiquantitative RT-PCR were used to confirm the accuracy of RNA-seq data. In total, nine of DEGs were selected, which are related to the regulation of skeletal development. The result of semiquantitative RT-PCR showed that mRNA expression levels of genes related to skeletal development were much higher in hindlimbs compared to the tail at Gs 42. (Fig. 7A,B). In addition, among all these genes, FGFBP3 and Ihh were most highly expressed in hindlimbs at Gs 42, and D2 and Sox9 were higher. In constrast, the expression of THα, THβ, D3, BMP6, and Wnt10b were lower in hindlimbs at Gs 42 (Fig. 7C). We also analyzed the nine genes expressed in hindlimbs among different developmental stages. qRT-PCR showed that the mRNA expression of TRα, TRβ, Wnt10b, BMP6, Ihh, Sox9, and FGFBP3 was down-regulated with the process of bones development (Fig. 7D). However, the D2 and D3 were up-regulated and peaked in hindlimbs at Gs 42, then down-regulated and bottomed out at Gs 46 (Fig. 7D).

In Situ Hybridization of Ihh

Ihh signaling has important roles in chondrogenesis and endochondral ossification. To identify the location of Ihh mRNA expression, we conducted in situ hybridization using sections prepared from hindlimbs of *B. gargarizans* over different stages. As shown in Figure 8, the expression of Ihh was abundant in prehypertrophic chondrocytes zone in hindlimbs at Gs 40, but its expression was not apparent in muscle cell adjacent to the growth cartilage (Fig. 8B). Positive signals for the Ihh mRNA were also observed in the outer periosteal region at Gs 40 (Fig. 8B). Similarly, Ihh mRNA were also found abundant in prehypertrophic chondrocytes zone in hindlimbs of *B. gargarizans* at Gs 42 and Gs 46 (Fig. 8E,F).

In Situ Hybridization of Sox9

To better understand the role of Sox9 in regulation of chondrocyte behavior in growth cartilage, we analyzed the expression of Sox9 in growth cartilage by in situ hybridization. In the hindlimbs of *B. gargarizans* at Gs 40, Sox9 was abundantly expressed in the columnar, prehypertrophic, and upper hypertrophic zones in the growth cartilage, while positive signals for the Sox9 mRNAs were not observed in muscle cell adjacent to the growth cartilage (Fig. 9B). Similar results were also observed in the growth cartilage of hindlimbs of *B. gargarizans* at Gs 42 and Gs 46 (Fig. 9D,F).

Discussion

The ossification of hindlimb bone exhibited a specific sequence, and endochondral ossification increased gradually during metamorphosis in *B. gargarizans*. Our results showed that the hindlimbs of *B. gargarizans* were ossified from proximal to distal, and ossification first began in the femur, then in tibiofibula, and finally in metatarsals. The majority of anurans shared the conservative patterns of hindlimb bone formation. For example, the hindlimbs of *Pseudis platensis* and *Rana pipiens* were also ossified from proximal to distal, and postaxial dominance occurred in the sequential formation of skeletal elements (Kemp and Hoyt, 1969; Fabrezi and Goldberg, 2009). On the other hand, endochondral ossification in hindlimbs of *B. gargarizans* increased gradually over metamorphosis. For example, the femur and the tibiofibula were ossified slightly at Gs 40 (about day 80 after fertilization), while they were ossified completely at Gs 42 (about day 2–3 after Gs 40). Even phalangeal formulae for the hindlimbs from toe III to toe V is formed at Gs 40; the metatarsals III–V were ossified slightly. Then the metatarsals III–V begin to fully ossify at Gs 42, and the metatarsals were fully ossified at Gs 46 (about day 2–3 after Gs 42). Due to its biological characteristics of ossification sequence and gradually increased endochondral ossification, the hindlimbs of *B. gargarizans* could be an ideal organ for exploring the molecular mechanisms of endochondral ossification.

In the present study, the transcriptomes of the hindlimbs and tail of *B. gargarizans* were constructed, and cDNA libraries were sequenced by using RNA-seq technology. We aimed to get candidate genes related to ossification of limbs by RNA-seq. A limitation of our study was that just a single biological sample was used in the RNA-seq. Also, it has been reported that the RNA-seq was carried out only from a single biological sample in several researches (Geng et al., 2017; Liu et al., 2017; Gardner et al., 2018; Singh et al., 2018). In the present study, on the basis of RNA-seq data, secondary and tertiary methods of analyses were used to validate the observed differences. In our study, a total of 3499 DEGs were identified, where expression of 2094 genes was up-regulated. Among these genes, 1201 genes were shown to be significantly up-regulated in the hindlimbs compared with those of the tail at Gs 42. It is well known that endochondral ossification occurs in limbs but not in tail during metamorphosis, because cartilage or bone is absent in the anuran tail. Thus, the up-regulated genes in hindlimbs might play critical roles in regulation of endochondral ossification. In addition, endochondral ossification in hindlimbs among different developmental stages was increased gradually in the order of Gs 40, Gs 42, and Gs 46; (40CH vs. 42CH) and 420 (42CH vs. 46CH) up-regulated genes were respectively identified. Our results indicated that the differences of genetic level reflected the ossification degree at different developmental stages. These data will provide us with powerful resources to further elucidate the molecular mechanisms of endochondral ossification in hindlimbs.

Earlier studies have demonstrated that endochondral ossification in mammal was regulated by systemic factors, locally secreted factors, and transcription factors (Nilsson et al., 2005; Ling et al., 2017). Thirty-two genes related to endochondral ossification (systemic factors, locally secreted factors, and transcription factors) were found, and the expression profiles of these genes were analyzed during the metamorphosis (Table 3). Systemic factors mainly included THs and GH, and locally secreted factors included Ihh, Wnts, BMPs, PTHrP, FGFs, and components of the cartilage extracellular matrix. Transcription factors included Runxs, Sox9, and MEF2C.

Thyroid hormones (THs), mainly T3 and T4, systemic factors, have been known to be important regulators of endochondral ossification (Waung et al., 2012). For example, T3 induces chondrocytes to enlarge into hypertrophic cells, as well as trigger death of hypertrophic cells by non-apoptotic modes of physiological death (Ballock and Reddi, 1994; Ahmed et al., 2007). THs level is regulated by iodothyronine deiodinases (D1, D2, and D3) via an outer-/inner-ring deiodination reaction. D1 and D2 are capable of converting T4 to T3 by 5' monodeiodination. By contrast, D3 converts T4 and T3 to less-active metabolites (Bianco et al., 2002; Bassett and Williams, 2003; Zoeller et al., 2007). In the present study, the mRNA of D2 was expressed at high levels in hindlimbs at premetamorphosis and peaked at metamorphic climax, then down-regulated at complete metamorphosis. Hence, high expression of D2 in hindlimbs at metamorphic climax led to a high level of T3, which enhanced hypertrophy and death of chondrocyte of endochondral ossification in hindlimbs.

Thyroid hormone receptors are nuclear receptors: Two thyroid hormone receptor genes exist (TRα and TRβ), which play an important role in endochondral ossification and the development of hindlimbs (Xing et al., 2014). For example, a research study for *Xenopus tropicalis* tadpoles has reported that knockout of TRα led to precocious hindlimb development with early increased expression of TH-response genes important for metamorphosis (Wen and Shi, 2015). TRβ knockout mice displayed advanced endochondral ossification and increased bone mineralization due to accelerated growth plate chondrocyte differentiation (O'Shea et al., 2005; Bassett et al., 2007; Wojcicka et al., 2013). In the present study, a gradual decrease of the mRNA of TRα and TRβ during metamorphosis was validated by RNA sequencing and qRT-PCR. Thus, lower expression of TRα and TRβ in hindlimbs at metamorphic climax and complete metamorphosis may increase the degree of endochondral ossification and enhance hindlimb growth.

During endochondral ossification, Ihh and PTHrP play important roles in early chondrocyte proliferation and differentiation (van Donkelaar and Huiskes, 2007). A study has demonstrated that Ihh and PTHrP regulate chondrocyte differentiation through the establishment of a negative-feedback mechanism (Vortkamp et al., 1996). Ihh induces the expression of PTHrP, which keeps chondrocytes in a proliferating state and negatively regulates the onset of hypertrophic differentiation (St-Jacques et al., 1999; Wongdee et al., 2013). In the present study, based on the RNA-seq data, the Ihh and PTHrP exhibited similar developmental expression patterns where they were expressed at high levels in

hindlimbs of *B. gargarizans* at premetamorphosis and then down-regulated at the end of metamorphosis. Additionally, the mRNA level of Ihh was validated by qRT-PCR, and the expression of Ihh was observed in prehypertrophic chondrocytes zone in hindlimbs of *B. gargarizans* by using in situ hybridization. Our result was consistent with Moriishi et al. (2005), who found that prehypertrophic chondrocytes located at the lower part of the growth cartilage in the limbs of *X. laevis* expressed Ihh mRNA. Therefore, the present observations confirmed that Ihh was positively correlated with PTHrP. High expression of Ihh and PTHrP at premetamorphosis could promote the chondrocyte proliferation, while lower mRNA levels of Ihh and PTHrP at metamorphosis climax contributed to the hypertrophic differentiation.

BMPs, subgroups of the transforming growth factor-β (TGFβ) superfamily, could induce bone formation. Several lines of evidence have demonstrated that BMPs can regulate the level of chondrocyte proliferation and differentiation (Minina et al., 2001). In addition, most BMPs, including BMP6 and BMP7, are able to stimulate osteogenesis in premature or mature osteoblasts (Brigaud et al., 2017). In the present study, the expression of BMP6 in hindlimbs of *B. gargarizans* was gradually increased during the metamorphosis, whereas BMP7 was decreased. It has been shown that BMP7 is expressed by proliferative chondrocytes and BMP6 is expressed by prehypertrophic and hypertrophic chondrocytes (van der Eerden et al., 2003). Therefore, we speculated that BMP7 may play an essential role in chondrocyte proliferation at early stage, and BMP6 may be involved in chondrocyte differentiation at later stage.

Sox9 is a master transcription factor that plays multiple roles in the regulation of chondrocyte behavior during endochondral ossification (Murakami et al., 2000). For example, Dy et al. (2012) has found that Sox9 maintained columnar proliferation, delayed prehypertrophy, and then prevented osteoblastic differentiation of chondrocytes by lowering β-catenin signaling and Runx2 expression. The study of Postlethwait et al. (2016) reported that genes encoding the key skeletogenesis regulatory factors Sox9 and Runx2 were expressed in a fashion similar to that of orthologs in numerous well mineralized fish. It has also been reported that Sox9 was required for chondrocyte hypertrophy (Ohba et al., 2015). In the present study, Sox9 expression in the hindlimbs of *B. gargarizans* was higher than most of the other selected genes, and the expression was up-regulated over the different stages. The mRNA level of Sox9 was also validated by qRT-PCR. In addition, Sox9 was expressed in the columnar, prehypertrophic, and upper hypertrophic zones in the growth cartilage by using in situ hybridization. The location of Sox9 in *B. gargarizans* was consistent with the results of experiments in *X. laevis* (Tazumi et al., 2010) and mice (Dy et al., 2012). Thus, Sox9 may play an essential role in multiple stages of the cartilage program from mesenchymal condensation to chondrocyte hypertrophy during amphibian metamorphosis.

Runx2 belongs to the Runx family of transcription factors and promotes the full progression of hypertrophic differentiation (Zelzer et al., 2001). Mice devoid of Runx2 completely lack osteoblasts and possess a skeleton made only of chondrocytes, while mice heterozygous for Runx2 have hypoplastic clavicles with delayed closure of the fontanelles (Komori et al., 1997). We found that the expression of Runx2 in hindlimbs of *B. gargarizans* was up-regulated gradually during the metamorphosis. It has been known that the expression of Runx2 was inhibited by PTHrP, and the activity of Runx2 was repressed by Sox9, which appears to contribute to the ability of PTHrP and Sox9 to delay chondrocyte hypertrophy (Guo et al., 2006; Dy et al., 2012). We thus suggest that gradual up-regulation of Runx2 may play an essential role in maintaining an appropriate balance between continued proliferation and progression to hypertrophy in chondrocytes in growth cartilage and the subsequent development of the skeletal system during amphibian metamorphosis.

Vascular endothelial growth factor (VEGF), a family of homodimeric proteins, is one of the most important regulators of vascular development and angiogenesis (Hoeben et al., 2004; Coultas et al., 2005). Also, VEGF plays critical roles in osteogenesis, since bone is a highly vascularized organ (Gerber et al., 1999; Hu and Olsen, 2016). During osteogenesis, VEGF is produced by osteoblast precursors, and this induces osteoblastic cells to migrate into the primary ossification center (Zelzer et al., 2002; Maes et al., 2010). Also, VEGF regulates surrounding muscles into either chondrocytes or osteoblasts (Kodama et al., 1991; Niida et al., 1999; Chan et al., 2015). In the present study, the expression of VEGF was present at metamorphic climax. In contrast, the expression of VEGF was absent at premetamorphosis and complete metamorphosis. These data indicate that differentiation of osteoblasts by VEGF may be necessary to endochondral ossification at metamorphic climax.

We provided an overview of the roles of systemic factors, locally secreted factors, and transcription factors in regulating endochondral ossification of *B. gargarizans* (Fig. 10) according to the review (Mackie et al., 2008). The molecular mechanisms regulating endochondral ossification in amphibians might be similar to those in mammals. Our study will provide a useful background for future study of endochondral ossification in amphibians.

Experimental Procedures

Animals

Three mating pairs of adult *B. gargarizans* collected in February 2017 from Qinling Mountains, Shaanxi Province, China, were held in one aquarium with shallow water (50 mm). After spawning, 150 embryos at Gs 3 were randomly assigned to three glass aquaria (50 cm × 20 cm × 20 cm) with 5 L dechlorinated water. All tanks were maintained at about 18 ± 1°C on a 12 h light/12 h dark regimen with continuous, gentle aeration. Test water was completely replaced every 48 h in all tanks. Embryos were not fed during exposure. After hatching, larvae were offered boiled lettuces. Animals used in this study were treated and maintained in accordance with the guidelines of the Laboratory Animal Care and Use Committee of Shaanxi Normal University and China Wildlife Conservation Association.

Determination of the Skeletal Development

To examine the developmental process of the skeleton through metamorphosis *in B. gargarizans*, the double-staining methodology was used to stain transparent specimen of larval skeletons. Three tadpoles per stage were euthanized with 1% buffered tricaine methanesulfonate at Gs 40, Gs 42, and Gs 46, respectively. Then larvae were decolorized with 30% H_2O_2 and defatted with acetone. After being eviscerated and cleared, each specimen was stained based on the methods of Alcian Blue-Alizarin Red double staining. Bones were stained in red and cartilages in blue. All

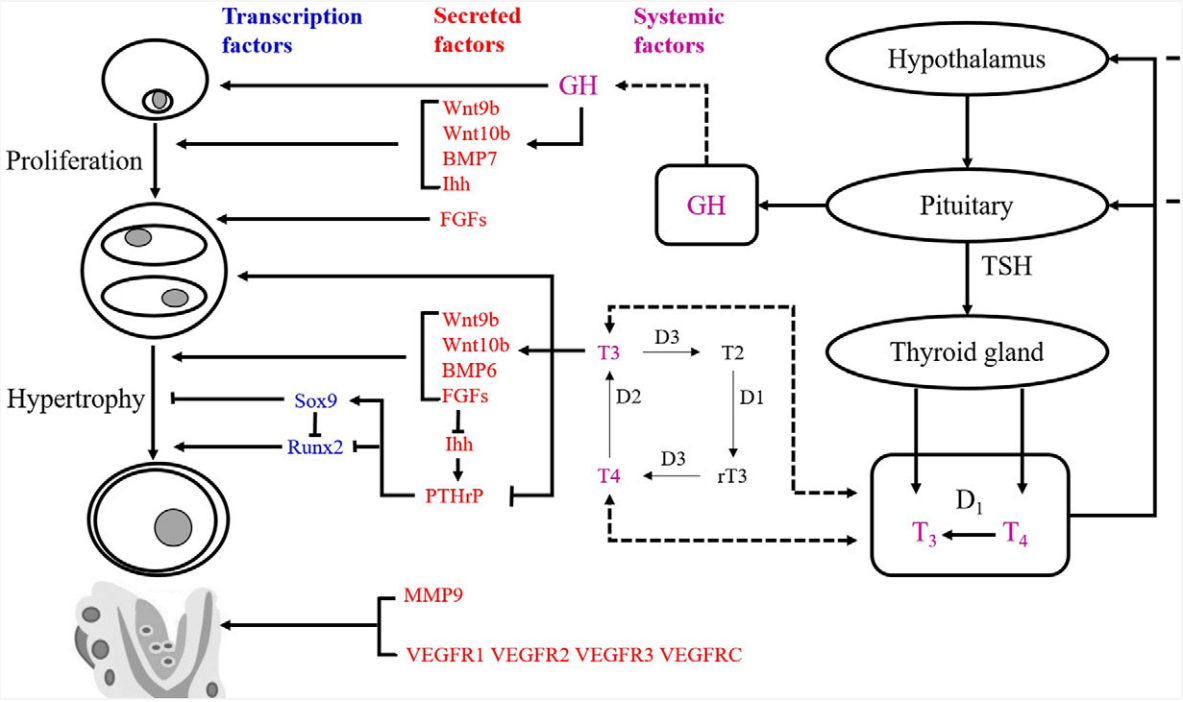

Fig. 10. Schematic diagram providing an overview of the roles of systemic factors (purple), locally secreted factors (red), and transcription factors (blue) in the regulation of chondrocyte proliferation and hypertrophy during endochondral ossification in *B. gargarizans*.

photos were taken under microscope Discovery.V12 with a computer and imaging system.

RNA Extraction and cDNA Library Preparation

Three *B. gargarizans* tadpoles per stage were randomly collected at Gs 40, Gs 42, and Gs 46, respectively. The tissues were sampled and pooled from the three tadpoles at each stage for constructing cDNA libraries. However, the RNA-seq was carried out only from a single biological sample for each stage/tissue due to the limitation of the number of test animals. It is well known that a key feature of tadpoles is the complete absence of caudal skeleton in the tail (Wassersug, 1989). Then, the tail was used as a negative control in contrast to the hindlimbs with skeleton. Total RNA was extracted from hindlimbs of *B. gargarizans* at Gs 40, Gs 42, and Gs 46 and from the tail at Gs 42 using E.Z.N.A. Tissue RNA Kit (Omega) according to the manufacturer's manual. RNA quality was assessed by spectrophotometry and electrophoresis on a 1.5% agarose gel with ethidium bromide-stained. RNA quantification was performed using NanoDrop instrument (Thermo) at 260 nm. The cDNA libraries were prepared using the Ovation RNA-seq System V2 (NuGEN) per the manufacturer's instructions, and the final product was assessed for its size distribution and concentration using Bioanalyzer High Sensitivity DNA Kit (Agilent) and KAPA Library Quantification Kit (Kapa Biosystems).

Transcriptome Sequencing, De Novo Assembly and Functional Annotation

The libraries were submitted to the Illumina HiSeq 2500 platform for sequencing by use of a paired-end sequencing strategy (2 × 150 bp). Before de novo assembly, the raw sequences were filtered to remove adaptor fragments, reads containing unknown nucleotide "N" over 5% and low-quality reads with more than 20% of Q value < 10 bases. Then, a de novo assembly strategy and downstream analysis were performed using Trinity (Grabherr et al., 2011; Haas et al., 2013). To annotate the assembled unigenes and predict function, they were aligned with BLASTX (Camacho et al., 2009) to the NCBI-nr, GO, COG, and KEGG databases with an E-value threshold of 1e−5. The classification of the unigenes into GO term categories was performed based on GO annotation results (Ye et al., 2006). In addition, the pathway analysis was performed using the KAAS webserver from KEGG (Kyoto Encyclopedia of Genes and Genomes) database, which could identify significantly metabolic pathways or signal transduction pathways (Kanehisa et al., 2014).

Differential Gene Expression Analysis

DEG libraries were constructed separately between tail and hindlimbs at Gs 42, and among hindlimbs of different developmental stages in *B. gargarizans*. Gene-expression levels were measured based on FPKM values (Mortazavi et al., 2008). Significance was accepted only at a false discovery rate (FDR) cutoff of 0.05 and Log_2 fold-change ($|Log_2FC|$)>1. The enrichment of GO results and KEGG pathway analysis of DEGs were then performed using a hypergeometric distribution (Conesa et al., 2005).

Quantitative Real-time RT-PCR Validation

qRT-PCR was conducted using SYBR Premix Ex Taq II (Tli RNaseH Plus) (TaKaRa; code No. RR820A) and CFX96 Real-Time Detection System (Bio-Rad) according to the manufacturer's instructions, with initial denaturation at 94°C for 3 min, followed by 30 cycles of denaturation at 94°C for 30 sec, annealing at 52°C for 30 sec, and extension at 72°C for 1min. A 1-μl cDNA template was included in a 25-μL PCR reaction with the

TABLE 4. The primers for amplification of the genes from *B. gargarizans* larvae

Target	Element	Sequence (5'-3')	Amplification length (bp)
D2	D2-S D2-AS	CGATCTTCTTGGTTTCTGT ATGTAGCCGACTTCCTCTT	115
D3	D3-S D3-AS	CCAACACGGAGGTGGTGAT TTGCAGGCGAGCCATGAAC	128
TRα	TRα-S TRα-AS	AAAACAGCTTGCAGCAGAG GTGGTGAGATGGCAGTGAA	139
TRβ	TRβ-S TRβ-AS	GACAGCGATACGCCTAAAT GATCATGTCACTCCGAGCC	150
Ihh	Ihh-S Ihh-AS	AGTCATTGATCCCTCTG ATCCAATCTCATACGGTCA	164
Sox9	Sox9-S Sox9-AS	AGTCAGGGTGAATGGATC GATGTTCATGGTCGGTGC	215
BMP6	BMP6-S BMP6-AS	TTCTTGCGGTTGCTTGTT AGTTTGAGGTCGGTAGGA	206
FGFBP3	FGFBP3-S FGFBP3-AS	TACCAAGGATCTGTCTCC AGTGAAAACGGTATGCGA	223
Wnt10b	Wnt10b-S Wnt10b-AS	CTGTTGGCTTGTCTTATT ATTGTCAGGCTTTCAGTC	196
β-actin	β-actin-S β-actin-AS	TGAAGAGCACCCTGTCCTAC CAGCCAAGTCAAGACGTAGA	123

following components: 1.0 μL each of forward and reverse primer; 12.5 μL of 2 × SYBR Premix Ex Taq II; and distilled water. Primers were designed using Primer Premier 5.0 software and were synthesized by Beijing Genomic Institute. Primer pair sequences and the expected sizes of PCR products are listed in Table 4. The mRNA expression level was measured by determining the cycle threshold (CT), which is the number of PCR cycles required for the fluorescence to exceed a value significantly higher than the background fluorescence (Wu et al., 2017).

Histological Analysis

Hindlimbs of the tadpoles at Gs 40, Gs 42, and Gs 46 were dissected under anesthesia with 0.1% ethyl-o-aminobenzoate and fixed for 12 h at 4°C in 4% paraformaldehyde solution in phosphate buffer (pH 7.4), respectively. Then specimens were processed for standard paraffin embedding. Six-micrometer-thick sections were cut and stained by hematoxylin and eosin (H&E). The sections were observed and photographed under Nikon ECLIPSE 80i Microscope equipped with a computer and imaging system.

In Situ Hybridization

To identify the location of Ihh and Sox9 mRNA expression, we conducted in situ hybridization using sections prepared from hindlimbs of *B. gargarizans* over different stages. The cDNA fragments of Ihh and Sox9 were subcloned into pGEM-T easy vector. After linearization with PstI, the plasmid was transcribed by T7 RNA polymerase using DIG RNA Labeling Kit (Roche) to produce a sense RNA probe. An antisense RNA probe was transcribed by Sp6 RNA polymerase after linearization with ApaI. Sense RNA probes were used in situ hybridization to confirm the specificity of the antisense RNA probe (data not shown). In situ hybridization was performed as described previously with a slight modification (Moriishi et al., 2005). After treatment with proteinase K (20 lg/ml) for 25 min at 37°C, the sections were incubated for 18 h at 37°C with a hybridization mixture, which consisted of 50% deionized formamide, 0.01M Tris/HCl (pH 7.4), 0.6 M NaCl, 1 mM EDTA (pH 7.4), 1 × Denhardt's solution, 15% dextran sulfate, 250 lg/ml yeast tRNA, and the probes (1 lg/ml).

Acknowledgments

We are grateful to Dr. Gang Wang from University of Kentucky for valuable suggestions and improving scientific writings.

References

Ahmed YA, Tatarczuch L, Pagel CN, Davies HM, Mirams M, Mackie EJ. 2007. Physiological death of hypertrophic chondrocytes. Osteoarthritis Cartilage 15:575–586.

Ballock RT, Reddi AH. 1994. Thyroxine Is the Serum Factor That Regulates Morphogenesis of Columnar Cartilage from Isolated Chondrocytes m Chelmeally Defined Medium. J Cell Biol 126: 1311–1318.

Banbury B, Maglia AM. 2006. Skeletal development of the Mexican spadefoot, Spea multiplicata (Anura: Pelobatidae). J Morphol 267: 803–821.

Bassett JH, Williams GR. 2003. The molecular actions of thyroid hormone in bone. Trends Endocrinol Metab 14:356–364.

Bassett JH, O'Shea PJ, Sriskantharajah S, Rabier B, Boyde A, Howell PG, Weiss RE, Roux JP, Malaval L, Clement-Lacroix P, Samarut J, Chassande O, Williams GR. 2007. Thyroid hormone excess rather than thyrotropin deficiency induces osteoporosis in hyperthyroidism. Mol Endocrinol 21:1095–1107.

Bianco AC, Salvatore D, Gereben B, Berry MJ, Larsen PR. 2002. Biochemistry, cellular and molecular biology, and physiological roles of the iodothyronine selenodeiodinases. Endocr Rev 23: 38–89.

Bird NC, Mabee PM. 2003. Developmental morphology of the axial skeleton of the zebrafish, Danio rerio (Ostariophysi: Cyprinidae). Dev Dyn 228:337–357.

Brigaud I, Agniel R, Leroy-Dudal J, Kellouche S, Ponche A, Bouceba T, Mihailescu N, Sopronyi M, Viguier E, Ristoscu C, Sima F, Mihailescu IN, Carreira ACO, Sogayar MC, Gallet O,

Anselme K. 2017. Synergistic effects of BMP-2, BMP-6 or BMP-7 with human plasma fibronectin onto hydroxyapatite coatings: A comparative study. Acta Biomater 55:481–492.
Brown DD, Cai L. 2007. Amphibian metamorphosis. Dev Biol 306: 20–33.
Camacho C, Coulouris G, Avagyan V, Ma N, Papadopoulos J, Bealer K, Madden TL. 2009. BLAST+: architecture and applications. BMC Bioinformatics 10:421.
Chan CKF, Seo EY, Chen JY, Lo D, McArdle A, Sinha R, Tevlin R, Seita J, Vincent-Tompkins J, Wearda T, Lu WJ, Senarath-Yapa K, Chung MT, Marecic O, Tran M, Yan KS, Upton R, Walmsley GG, Lee AS, Sahoo D, Kuo CJ, Weissman IL, Longaker MT. 2015. Identification and Specification of the Mouse Skeletal Stem Cell. Cell 160:285–298.
Conesa A, Gotz S, Garcia-Gomez JM, Terol J, Talon M, Robles M. 2005. Blast2GO: a universal tool for annotation, visualization and analysis in functional genomics research. Bioinformatics 21: 3674–3676.
Coultas L, Chawengsaksophak K, Rossant J. 2005. Endothelial cells and VEGF in vascular development. Nature 438:937–945.
Dy P, Wang W, Bhattaram P, Wang Q, Wang L, Ballock RT, Lefebvre V. 2012. Sox9 directs hypertrophic maturation and blocks osteoblast differentiation of growth plate chondrocytes. Dev Cell 22:597–609.
Erdmann K. 1933. Zur Entwicklung des knöchernen Skelets von Triton und Rana unter besonderer Berücksichtigung der Zeitfolge der Ossifikationen. Z Anat Entwicklungs 101: 566–651.
Fabrezi M, Goldberg J. 2009. Heterochrony During Skeletal Development of Pseudis platensis (Anura, Hylidae) and the Early Offset of Skeleton Development and Growth. J Morphol 270:205–220.
Gao L, Wang H, Liang G. 2015. Development and ossification sequence of the hind limb during metamorphosis of bufo gargarizans tadpoles. Sichuan Journal of Zoology 34:345–351.
Gardner M, Dhroso A, Johnson N, Davis EL, Baum TJ, Korkin D, Mitchum MG. 2018. Novel global effector mining from the transcriptome of early life stages of the soybean cyst nematode Heterodera glycines. Sci Rep 8:2505.
Geng X, Li W, Shang H, Gou Q, Zhang F, Zang X, Zeng B, Li J, Wang Y, Ma J, Guo J, Jian J, Chen B, Qiao Z, Zhou M, Wei H, Fang X, Xu C. 2017. A reference gene set construction using RNA-seq of multiple tissues of Chinese giant salamander, Andrias davidianus. Gigascience 6:1–7.
Gerber HP, Vu TH, Ryan AM, Kowalski J, Werb Z, Ferrara N. 1999. VEGF couples hypertrophic cartilage remodeling, ossification and angiogenesis during endochondral bone formation. Nat Med 5:623–628.
Gómez RO, Regueira E, O'Donohoe MEA, Hermida GN. 2017. Delayed osteogenesis and calcification in a large true toad with a comparative survey of the timing of skeletal ossification in anurans. Zool Anz 267:101–110.
Gosner KL. 1960. A Simplified Table for Staging Anuran Embryos and Larvae with Notes on Identification. Herpetologica 16:183–190.
Grabherr MG, Haas BJ, Yassour M, Levin JZ, Thompson DA, Amit I, Adiconis X, Fan L, Raychowdhury R, Zeng Q, Chen Z, Mauceli E, Hacohen N, Gnirke A, Rhind N, di Palma F, Birren BW, Nusbaum C, Lindblad-Toh K, Friedman N, Regev A. 2011. Full-length transcriptome assembly from RNA-Seq data without a reference genome. Nat Biotechnol 29:644–652.
Guo J, Chung UI, Yang D, Karsenty G, Bringhurst FR, Kronenberg HM. 2006. PTH/PTHrP receptor delays chondrocyte hypertrophy via both Runx2-dependent and -independent pathways. Dev Biol 292:116–128.
Haas A. 1999. Larval and metamorphic skeletal development in the fast-developing frog Pyxicephalus adspersus, (Anura, Ranidae). Zoomorphology 119:23–35.
Haas BJ, Papanicolaou A, Yassour M, Grabherr M, Blood PD, Bowden J, Couger MB, Eccles D, Li B, Lieber M, MacManes MD, Ott M, Orvis J, Pochet N, Strozzi F, Weeks N, Westerman R, William T, Dewey CN, Henschel R, LeDuc RD, Friedman N, Regev A. 2013. De novo transcript sequence reconstruction from RNA-seq using the Trinity platform for reference generation and analysis. Nat Protoc 8:1494–1512.
Hoeben A, Landuyt B, Highley MS, Wildiers H, Van Oosterom AT, De Bruijn EA. 2004. Vascular endothelial growth factor and angiogenesis. Pharmacol Rev 56:549–580.
Hu K, Olsen BR. 2016. The roles of vascular endothelial growth factor in bone repair and regeneration. Bone 91:30–38.
Kanehisa M, Goto S, Sato Y, Kawashima M, Furumichi M, Tanabe M. 2014. Data, information, knowledge and principle: back to metabolism in KEGG. Nucleic Acids Res 42:D199–205.
Karp SJ, Schipani E, St-Jacques B, Hunzelman J, Kronenberg H, McMahon AP. 2000. Indian hedgehog coordinates endochondral bone growth and morphogenesis via parathyroid hormone related-protein-dependent and -independent pathways. Development 127:543–548.
Kemp NE, Hoyt JA. 1969. Sequence of ossification in the skeleton of growing and metamorphosing tadpoles of Rana pipiens. J Morphol 129:415–443.
Kodama H, Yamasaki A, Nose M, Niida S, Ohgame Y, Abe M, Kumegawa M, Suda T. 1991. Congenital Osteoclast Deficiency in Osteopetrotic (Op/Op) Mice Is Cured by Injections of Macrophage Colony-Stimulating Factor. J Exp Med 173:269–272.
Komori T, Yagi H, Nomura S, Yamaguchi A, Sasaki K, Deguchi K, Shimizu Y, Bronson RT, Gao YH, Inada M, Sato M, Okamoto R, Kitamura Y, Yoshiki S, Kishimoto T. 1997. Targeted disruption of Cbfa1 results in a complete lack of bone formation owing to maturational arrest of osteoblasts. Cell 89:755–764.
Kulkarni PS, Gramapurohit NP. 2017. Effect of corticosterone on larval growth, antipredator behaviour and metamorphosis of Hylarana indica. Gen Comp Endocrinol 251:21–29.
Ling IT, Rochard L, Liao EC. 2017. Distinct requirements of wls, wnt9a, wnt5b and gpc4 in regulating chondrocyte maturation and timing of endochondral ossification. Dev Biol 421:219–232.
Liu W, Chen M, Bai L, Zhuang Z, Fan C, Jiang N, Zhao J, Ma S, Xiang X. 2017. Comprehensive transcriptomics and proteomics analyses of pollinated and parthenocarpic litchi (Litchi chinensis Sonn.) fruits during early development. Sci Rep 7:5401.
Mackie EJ, Ahmed YA, Tatarczuch L, Chen KS, Mirams M. 2008. Endochondral ossification: how cartilage is converted into bone in the developing skeleton. Int J Biochem Cell Biol 40:46–62.
Maes C, Kobayashi T, Selig MK, Torrekens S, Roth SI, Mackem S, Carmeliet G, Kronenberg HM. 2010. Osteoblast Precursors, but Not Mature Osteoblasts, Move into Developing and Fractured Bones along with Invading Blood Vessels. Dev Cell 19:329–344.
Minina E, Wenzel HM, Kreschel C, Karp S, Gaffield W, McMahon AP, Vortkamp A. 2001. BMP and Ihh/PTHrP signaling interact to coordinate chondrocyte proliferation and differentiation. Development 128:4523–4534.
Moriishi T, Shibata Y, Tsukazaki T, Yamaguchi A. 2005. Expression profile of Xenopus banded hedgehog, a homolog of mouse Indian hedgehog, is related to the late development of endochondral ossification in Xenopus laevis. Biochem Biophys Res Commun 328: 867–873.
Mortazavi A, Williams BA, McCue K, Schaeffer L, Wold B. 2008. Mapping and quantifying mammalian transcriptomes by RNA-Seq. Nat Methods 5:621–628.
Murakami S, Kan M, McKeehan WL, De CB. 2000. Up-regulation of the chondrogenic sox9 gene by fibroblast growth factors is mediated by the mitogen-activated protein kinase pathway. Proc Natl Acad Sci U S A 97:1113–1118.
Nakai Y, Nakajima K, Robert J, Yaoita Y. 2016. Ouro proteins are not essential to tail regression during Xenopus tropicalis metamorphosis. Genes Cells 21:275–286.
Niida S, Kaku M, Amano H, Yoshida H, Kataoka H, Nishikawa S, Tanne K, Maeda N, Nishikawa SI, Kodama H. 1999. Vascular endothelial growth factor can substitute for macrophage colony-stimulating factor in the support of osteoclastic bone resorption. J Exp Med 190:293–298.
Nilsson O, Marino R, De Luca F, Phillip M, Baron J. 2005. Endocrine regulation of the growth plate. Horm Res 64:157–165.
Nishimura R, Hata K, Ono K, Amano K, Takigawa Y, Wakabayashi M, Takashima R, Yoneda T. 2012. Regulation of endochondral ossification by transcription factors. Front Biosci (Landmark Ed) 17:2657–6266.
Ohba S, He X, Hojo H, McMahon AP. 2015. Distinct Transcriptional Programs Underlie Sox9 Regulation of the Mammalian Chondrocyte. Cell Rep 12:229–243.
O'Shea PJ, Bassett JH, Sriskantharajah S, Ying H, Cheng SY, Williams GR. 2005. Contrasting skeletal phenotypes in mice with

an identical mutation targeted to thyroid hormone receptor alpha1 or beta. Mol Endocrinol 19:3045–3059.
Postlethwait JH, Yan YL, Desvignes T, Allard C, Titus T, Le François NR, Detrich HW 3rd. 2016. Embryogenesis and early skeletogenesis in the antarctic bullhead notothen, Notothenia coriiceps. Dev Dyn 245:1066–1080.
Robinson MD, McCarthy DJ, Smyth GK. 2010. edgeR: a Bioconductor package for differential expression analysis of digital gene expression data. Bioinformatics 26:139–140.
Singh J, Kalberer SR, Belamkar V, Assefa T, Nelson MN, Farmer AD, Blackmon WJ, Cannon SB. 2018. A transcriptome-SNP-derived linkage map of Apios americana, (potato bean) provides insights about genome re-organization and synteny conservation in the phaseoloid legumes. Theor Appl Genet 131:333–351.
St-Jacques B, Hammerschmidt M, McMahon AP. 1999. Indian hedgehog signaling regulates proliferation and differentiation of chondrocytes and is essential for bone formation. Genes Dev 13:2072–2086.
Sun T, Zhan B, Gao Y. 2015. A novel cathelicidin from Bufo bufo gargarizans Cantor showed specific activity to its habitat bacteria. Gene 571:172–177.
Tazumi S, Yabe S, Uchiyama H. 2010. Paraxial T-box genes, Tbx6 and Tbx1, are required for cranial chondrogenesis and myogenesis. Dev Biol 346:170–180.
van der Eerden BC, Karperien M, Wit JM. 2003. Systemic and local regulation of the growth plate. Endocr Rev 24:782–801.
van Donkelaar CC, Huiskes R. 2007. The PTHrP-Ihh feedback loop in the embryonic growth plate allows PTHrP to control hypertrophy and Ihh to regulate proliferation. Biomech Model Mechanobiol 6:55–62.
Vortkamp A, Lee K, Lanske B, Segre GV, Kronenberg HM, Tabin CJ. 1996. Regulation of rate of cartilage differentiation by Indian hedgehog and PTH-related protein. Science 273:613–622.
Wang YH, Keenan SR, Lynn J, McEwan JC, Beck CW. 2015. Gremlin1 induces anterior-posterior limb bifurcations in developing Xenopus limbs but does not enhance limb regeneration. Mech Dev 138 Pt 3:256–267.
Wassersug RJ. 1989. Locomotion in Amphibian Larvae (or "Why Aren't Tadpoles Built Like Fishes?"). Integr Comp Biol 29:65–84.
Waung JA, Bassett JH, Williams GR. 2012. Thyroid hormone metabolism in skeletal development and adult bone maintenance. Trends Endocrinol Metab 23:155–162.
Wen L, Shi YB. 2015. Unliganded thyroid hormone receptor alpha controls developmental timing in Xenopus tropicalis. Endocrinology 156:721–734.
Wiens JJ. 1989. Ontogeny of the skeleton of Spea bombifrons (Anura: Pelobatidae). J Morphol 202:29–51.
Wojcicka A, Bassett JH, Williams GR. 2013. Mechanisms of action of thyroid hormones in the skeleton. Biochim Biophys Acta 1830: 3979–3986.
Wongdee K, Thonapan N, Saengamnart W, Krishnamra N, Charoenphandhu N. 2013. Bromocriptine modulates the expression of PTHrP receptor, Indian hedgehog, and Runx2 proteins in the growth plate of lactating rats. Mol Cell Biochem 381:191–199.
Wu C, Zhang Y, Chai L, Wang H. 2017. Histological changes, lipid metabolism and oxidative stress in the liver of Bufo gargarizans exposed to cadmium concentrations. Chemosphere 179:337–346.
Xing W, Cheng S, Wergedal J, Mohan S. 2014. Epiphyseal chondrocyte secondary ossification centers require thyroid hormone activation of Indian hedgehog and osterix signaling. J Bone Miner Res 29:2262–2275.
Yang L, Tsang KY, Tang HC, Chan D, Cheah KSE. 2014. Hypertrophic chondrocytes can become osteoblasts and osteocytes in endochondral bone formation. Proc Natl Acad Sci U S A 111: 12097–12102.
Ye J, Fang L, Zheng H, Zhang Y, Chen J, Zhang Z, Wang J, Li S, Li R, Bolund L, Wang J. 2006. WEGO: a web tool for plotting GO annotations. Nucleic Acids Res 34:W293–297.
Zelzer E, Glotzer DJ, Hartmann C, Thomas D, Fukai N, Soker S, Olsen BR. 2001. Tissue specific regulation of VEGF expression during bone development requires Cbfa1/Runx2. Mech Dev 106:97–106.
Zelzer E, McLean W, Ng YS, Fulkai N, Reginato AM, Lovejoy S, D'Amore PA, Olsen BR. 2002. Skeletal defects in VEGF (120/120) mice reveal multiple roles for VEGF in skeletogenesis. Development 129:1893–1904.
Zhou X, von der Mark K, Henry S, Norton W, Adams H, de Crombrugghe B. 2014. Chondrocytes Transdifferentiate into Osteoblasts in Endochondral Bone during Development, Postnatal Growth and Fracture Healing in Mice. PLoS Genet 10:e1004820.
Zoeller RT, Tan SW, Tyl RW. 2007. General background on the hypothalamic-pituitary-thyroid (HPT) axis. Crit Rev Toxicol 37: 11–53.